Journal of Engineering Mathematics 18 (1984) 89–103
© 1984 Martinus Nijhoff Publishers, The Hague. Printed in The Netherlands

On laminar steady flow in sinusoidal channels *

S. TSANGARIS [1] and E. LEITER [2]

[1] *National Technical University of Athens, Chair of Fluid Mechanics and Turbomachinery, 42 October 28th Avenue, Athens, Greece*

[2] *Abteilung Magnetohydrodynamik und Bioströmungsmechanik, Technische Universität Wien, Argentinierstrasse 8, A-1040 Wien, Austria*

(Received February 26, 1982 and in final form April 4, 1983)

Summary

In the present paper a perturbation method is developed in order to study viscous laminar flows through wavy-walled channels. The stream function of the flow is expanded in a series thereby the wall amplitude being the perturbation parameter. The walls of the channel are transformed into parallel straight lines in order to simplify the boundary conditions of the problem on the wall. Flow field and wall-shear stresses are calculated numerically up to the first perturbation order.

The position of the beginning separation on the channel walls and the associated critical Reynolds number are determined, as well as the extension of the region of the separated flow. The position of separation and reattachment points are given as functions of Reynolds numbers lying above the critical Reynolds number. The results are discussed and compared with the experimental results of other papers and further theoretical analysis.

1. Introduction

Viscous flow past wavy boundaries has attracted considerable interest in the last years because of the important role which it plays in several phenomena: the generation of wind waves on water, the formation of sedimentary ripples in river channels and dunes in deserts, the stability of a liquid film in contact with a gas stream, the rippling of melting surfaces, the transpiration cooling of re-entry vehicles and rocket boosters, cross hatching on ablative surfaces and film vaporization in combustion chambers. Physiologists and technicians are interested in it trying to explain blood and urinary flow and to apply the results in order to optimize artificial organs. The laminar flow in channels and pipes confined by wavy walls has nevertheless not been studied extensively.

Viscous flow in sinusoidally varying channels and pipes – peristaltic motions included – was treated by Burnes and Parkes [2] under the assumption that the Reynolds number is small enough for the Stokes approximation to be valid (inertial forces negligible in comparison with viscous forces). They got a solution by expressing the stream function as a Fourier cosine series determining the coefficients by assuming small values of the amplitude. The subsequent approximation in their analysis satisfying the boundary no-slip condition at the walls was replaced by Tsangaris and Leiter [16] by expressing the stream

* Supported by "Fonds zur Förderung der wissenschaftlichen Forschung", Vienna, Austria, Project Number 3214.

function as a Fourier series not in the physical plane but in a transformed plane where the wavy boundary is transformed into a straight one. The proposed analytical perturbation method for creeping flow through small-amplitude sinusoidal channels is extended to laminar flow with Reynolds numbers far above that for creeping flow in this paper. Steady and unsteady flow through furrowed channels has been studied numerically by Sobey [10]. He especially concentrated on the Reynolds-number effect, also for separated flow. The underlying concept of multistructured boundary layers as developed by Stewartson [12,13,14] yields a relation between the geometric parameters and Reynolds number for which separation occurs. Stephanoff, Sobey and Bellhouse [11] compared the results of Sobey's calculations with experiments observed by visualization techniques. (Final discussion in this paper refers to these two papers.) Fluid flow connected with heat transfer in wavy channels was calculated by Vajravelu [17] by a perturbation method for long-wave channels and by solving the obtained linear differential equations numerically. Forrester and Young [5] and Young and Tsai [18] theoretically and experimentally worked out the flow patterns in a (axisymmetric) stenosis determining also the Reynolds-number effect on the flow separation. Talukder et al. [15] studied the pressure losses in multiple stenoses and the associated flow patterns for the stream lines and the separating zones. (Discussion refers to these papers by Forrester, Young, Tsai and Talukder et al.)

The viscous flow of a liquid in a circular pipe whose radius has a slight sinusoidal variation was treated by Belinfante [1]. He calculated solutions numerically by power series. Manton [8] worked out the steady laminar flow for low Reynolds numbers in slowly-varying axisymmetric tubes of arbitrary radius variation. That means for sinusoidally varying tubes a long-wave approximation. His analytical perturbation solution yields some important result concerning the variation of the shear stresses and the flow separation. Some interesting experimental insight in the variation of the pressure and shear stresses along a wavy pipe for turbulent non-separated flow was given by Hsu and Kennedy [7]. A numerical treatment of the steady laminar separated flow in pipes with sinusoidal wall variation is presented in the paper of Chow and Soda [4]. The unsteady oscillatory viscous flow in pipes and channels of slowly-varying cross section has been calculated by Rao and Devanathan [9], by Hall [6] and by Cheng, Clark and Peng [3].

2. Formulation of the problem

Steady laminar flow of an incompressible Newtonian fluid in a symmetrically furrowed channel in terms of the stream function Ψ' is governed by the equation derived from the vorticity equation

$$\frac{\partial \Psi'}{\partial y'} \frac{\partial \Delta \Psi'}{\partial x'} - \frac{\partial \Psi'}{\partial x'} \frac{\partial \Delta \Psi'}{\partial y'} = \nu \Delta \Delta \Psi', \tag{1}$$

where

$$\Delta \equiv \nabla^2 \equiv \frac{\partial^2}{\partial x'^2} + \frac{\partial^2}{\partial y'^2}$$

and ν is the kinematic viscosity of the fluid. The symbols x', y' denote respectively the coordinates along and normal to the axis of the channel (see Fig. 1). The velocity

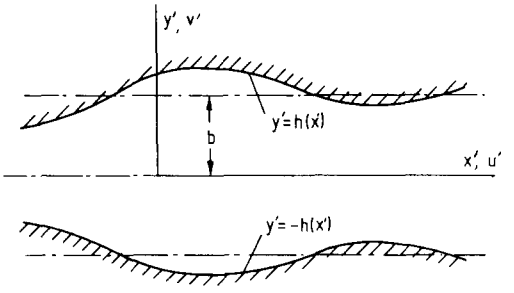

Figure 1. Geometry of a symmetric furrowed channel.

components along the x'- and y'-axis are respectively:

$$u' = \frac{\partial \Psi'}{\partial y'}, \qquad v' = -\frac{\partial \Psi'}{\partial x'}. \tag{2}$$

The boundary condition is the no-slip condition on the wall; symmetry with respect to x' – axis is to be added:

$$u' = \Psi'_{y'}(x', \pm h(x')) = 0, \qquad v' = -\Psi'_{x'}(x', \pm h(x')) = 0, \tag{3}$$

$$u'(x', y') = u'(x', -y'), \qquad v'(x', y') = -v'(x', -y'), \tag{4}$$

whereby the boundaries of the symmetric channel are given by

$$y' = \pm h(x'). \tag{5}$$

The shear stress at the wall boundary is (μ dynamic viscosity)

$$\tau' = \mu\left[\frac{1 - h_{x'}^2}{1 + h_{x'}^2}\left(\frac{\partial u'}{\partial y'} + \frac{\partial v'}{\partial x'}\right) + \frac{2h_{x'}}{1 + h_{x'}^2}\left(\frac{\partial v'}{\partial y'} - \frac{\partial u'}{\partial x'}\right)\right] \tag{6}$$

We introduce nondimensional variables

$$x = \frac{x'}{b}, \qquad y = \frac{y'}{b}, \qquad \Psi = \frac{\Psi'}{Ub}, \tag{7}$$

where b is the characteristic length according to Fig. 1 and U is the characteristic velocity along the x'-coordinate. Equation (1) then becomes

$$\mathrm{Re}\left(\frac{\partial \Psi}{\partial y}\frac{\partial \Delta\Psi}{\partial x} - \frac{\partial \Psi}{\partial x}\frac{\partial \Delta\Psi}{\partial y}\right) = \frac{\partial^4 \Psi}{\partial x^4} + 2\frac{\partial^4 \Psi}{\partial x^2 \partial y^2} + \frac{\partial^4 \Psi}{\partial y^4}. \tag{8}$$

Re is the Reynolds number of the flow given by

$$\mathrm{Re} = Ub/\nu, \tag{9}$$

where b is the channel half-gap. The nondimensional shear stress

$$\tau = \tau' \frac{b}{U\rho\nu} \tag{10}$$

then takes the nondimensional form

$$\tau = \left[\frac{1 - h_x^2}{1 + h_x^2} (\Psi_{yy} - \Psi_{xx}) - \frac{4h_x}{1 + h_x^2} \Psi_{xy} \right]. \tag{11}$$

In order to satisfy the boundary conditions on the wall we transform the independent variables x and y into η, ζ by

$$\eta = x, \qquad \zeta = \frac{y}{h(x)}. \tag{12}$$

Then the channel is transformed to a channel confined by parallel walls as shown in Fig. 2,

$$\zeta = \pm 1. \tag{13}$$

The equation (8) then transforms into

$$\mathrm{Re}\, \frac{1}{h} \left(\frac{\partial \Psi}{\partial \zeta} \frac{\partial \bar{\Delta} \Psi}{\partial \eta} - \frac{\partial \Psi}{\partial \eta} \frac{\partial \bar{\Delta} \Psi}{\partial \zeta} \right) = \bar{\Delta} \bar{\Delta} \Psi, \tag{14}$$

where $\bar{\Delta}$ is the Δ-operator transformed in η, ζ-variables,

$$\bar{\Delta} \equiv \frac{\partial^2}{\partial \eta^2} + \frac{1}{h^2} \left(h_\eta^2 \zeta^2 + 1 \right) \frac{\partial^2}{\partial \zeta^2} - 2\zeta \frac{h_\eta}{h} \frac{\partial^2}{\partial \eta \partial \zeta} + \zeta \frac{1}{h^2} \left(2h_\eta^2 - h h_{\eta\eta} \right) \frac{\partial}{\partial \zeta}. \tag{15}$$

The boundary condition on the wall turns out to be:

$$\Psi_\zeta = 0, \qquad \Psi_\eta = 0 \qquad \text{on} \quad \zeta = \pm 1. \tag{16}$$

The condition of the symmetric flow leads to

$$\Psi(\eta, -\zeta) = -\Psi(\eta, -\zeta) \tag{17}$$

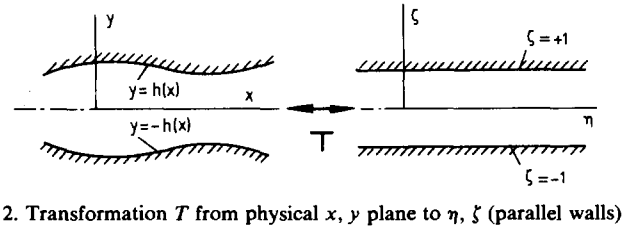

Figure 2. Transformation T from physical x, y plane to η, ζ (parallel walls) plane.

and the shear stress at the wall can be written in η, ζ-variables as

$$\tau = \Psi_{\zeta\zeta}\frac{\left(1-h_\eta^2\right)^2}{h^2\left(1+h_\eta^2\right)} - \Psi_{\eta\eta}\frac{1-h_\eta^2}{1+h_\eta^2} - 2\Psi_{\eta\zeta}\frac{h_\eta}{h} + \Psi_\zeta\left(\frac{h_{\eta\eta}}{h}-2\right)\frac{1}{1+h_\eta^2}. \tag{18}$$

3. Method of solution

We use the method of small perturbations to obtain analytical solutions of the problem for weakly-furrowed channels with boundary shape

$$h(\eta) = 1 + \epsilon f(\eta). \tag{19}$$

The solution of the governing equation is expanded in series in terms of the geometric parameter ϵ, and the asymptotic solution of Ψ is sought in the limit of $\epsilon \to 0$:

$$\Psi = \Psi_0 + \epsilon\Psi_1 + \ldots \tag{20}$$

By substitution of Eqn. (20) into Eqn. (14) and subsequent collection of terms with equal powers of ϵ, we get the following set of perturbation equations up to first-order results: zeroth order:

$$\Psi_{0\zeta\zeta\zeta\zeta} = 0, \tag{21a}$$

$$\Psi_{0\zeta}(\pm 1) = 0, \qquad \Psi_{0\eta}(\pm 1) = 0, \tag{21b}$$

first order:

$$\Psi_{1\eta\eta\eta\eta} + 2\Psi_{1\eta\eta\zeta\zeta} + \Psi_{1\zeta\zeta\zeta\zeta} + 12\zeta f_{\eta\eta} - \zeta\left(1-\zeta^2\right)f_{\eta\eta\eta\eta} =$$

$$\mathrm{Re}\left\{\left(1-\zeta^2\right)\left[\Psi_{1\eta\eta\eta} + \Psi_{1\zeta\zeta\eta} + 4\zeta f_\eta - \zeta\left(1-\zeta^2\right)f_{\eta\eta\eta}\right] + 2\Psi_{1\eta}\right\}, \tag{22a}$$

$$\Psi_{1\zeta}(\pm 1) = 0, \qquad \Psi_{1\eta}(\pm 1) = 0. \tag{22b}$$

From Eqns. (21a) and (21b) we obtain for the zeroth order the well-known Poiseuille-solution, not in the physical but in the transformed η, ζ-plane:

$$\Psi_0 = \zeta - \frac{\zeta^3}{3}. \tag{23}$$

This result has been noticed by many authors (see Manton [8]). In order to find analytical solutions for the first-order equation we continue our analysis for sinusoidal walls:

$$f(\eta) = -(\cos\eta + 1). \tag{24}$$

Substituting

$$\Psi_1(\zeta, \eta) = \left[g_1^*(\zeta) - \zeta(1-\zeta^2) \right] \cos \eta + g_2(\zeta) \sin \eta = g_1(\zeta) \cos \eta + g_2(\zeta) \sin \eta \quad (25)$$

and applying the method of separation of variables, a system of ordinary differential equations for the functions $g_1^*(\zeta)$ and $g_2(\zeta)$ is obtained:

$$g_{1\zeta\zeta\zeta\zeta}^* - 2g_{1\zeta\zeta}^* + g_1^* = \mathrm{Re}\left[(1-\zeta^2)(g_{2\zeta\zeta} - g_2) + 2g_2 \right], \quad (26a)$$

$$g_{2\zeta\zeta\zeta\zeta} - 2g_{2\zeta\zeta} + g_2 = -\mathrm{Re}\left[(1-\zeta^2)(g_{1\zeta\zeta}^* - g_1^*) + 2g_1^* \right]. \quad (26b)$$

The boundary condition equations (22b) lead to

$$g_1^*(\pm 1) = 0, \qquad g_{1\zeta}^*(\pm 1) = -2, \qquad g_2(\pm 1) = 0, \qquad g_{2\zeta}(\pm 1) = 0. \quad (27)$$

The system of Eqns. (26a) and (26b) will be solved numerically in order to determine the functions $g_1^*(\zeta)$ and $g_2(\zeta)$.

4. Solution and results

The system of Eqns. (26a) and (26b) subject to the boundary conditions (27) is a linear system of differential equations with two unknown functions and with variable coefficients. The boundary conditions are prescribed at both boundaries, $\zeta = +1$ and $\zeta = -1$, as function values and the values of its first-order derivatives. The above system is solved numerically using a finite-difference method. A regular mesh of equidistant points is used. The resulting system of linear equations is solved iteratively by block relaxation using a tridiagonal solver routine.

In Fig. 3 we see the numerical results of the functions $g_1^*(\zeta)$ and $g_2(\zeta)$ for Re = 1.0 and Re = 10. In the same figure are shown also the analytical results,

$$g_1^*(\zeta) = \frac{2}{\cosh 1 \sinh 1 - 1} (\sinh \zeta \cosh 1 - \zeta \cosh \zeta \sinh 1), \quad (28a)$$

$$g_2(\zeta) = 0 \quad (28b)$$

obtained by Tsangaris and Leiter [16] for the case of creeping flow at Re = 0. The curves for Re = 0 fit with an excellent accuracy to those for Re = 1.0. The same good agreement is valid also for the second derivatives of the functions $g_{1\zeta\zeta}^*(\pm 1)$ and $g_{2\zeta\zeta}(\pm 1)$ at the boundaries, which are dominant for the determination of the shear stress at the wall. It is for instance: $g_{1\zeta\zeta}^*(+1) = -6.791$, $g_{2\zeta\zeta}(+1) = 0$ for Re = 0 (analytical perturbation theory) and $g_{1\zeta\zeta}^*(+1) = -6.791$, $g_{2\zeta\zeta}(+1) = 0.015$ for Re = 0.1 (numerical solution). The second derivatives of the functions g_1^* and g_2 at the wall boundary $\zeta = +1$ are plotted in Fig. 4 as functions of the Reynolds number, Re.

In Figs. 5 to 9 the velocity profiles u and v in a channel with sinusoidal walls are shown, $\epsilon = 0.2$, at Reynolds numbers Re = 1.0, 10, 75, 200, 400. The velocity profiles are plotted at cross sections of the channel $x = 0$, 1, 2, 3, 4, 5 and 6.

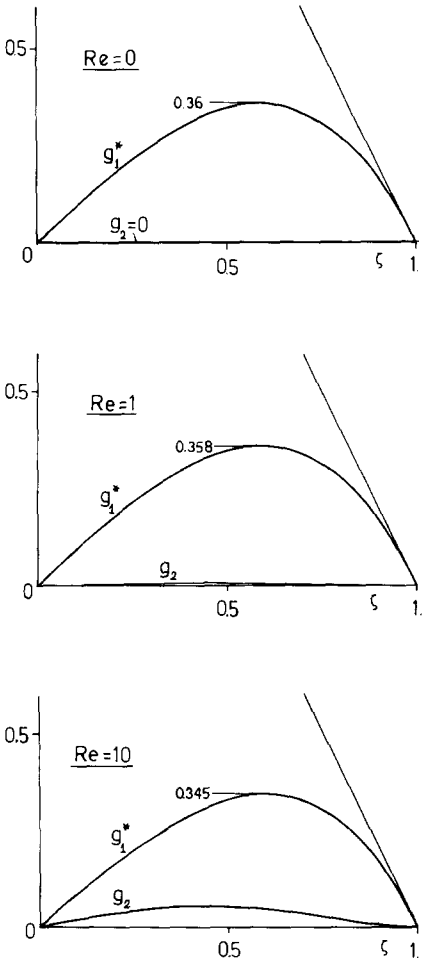

Figure 3. Analytical calculations of functions g_1^* and g_2 for Re = 0, [16], and numerical calculations for Re = 1 and Re = 10.

For small Reynolds numbers, for instance Re = 1, Re = 10, the viscous effects dominate the inertial ones. For larger Reynolds numbers, e.g. Re = 75, an influence of the velocity profile from the fluid inertia is evident. In the diverging part of the channel the u-profiles are flattened at the centerline. The flow becomes more asymmetric in symmetrically-lying cross sections of the converging and the diverging parts of the channel, regarding the distribution of u- and v-components of the velocity. The negative sign of the v-component for $x = 0$ and the positive sign of the same component for $x = \pi$ give a clear demonstration of the effect of inertia.

For Re = 200 the flow separation is just in way. The u-velocity profile approaches tangentially to y-planes near the wall and back flow in some cross sections of the channel is registrated.

For Re = 400 a separation bubble is recognized, as the back flow becomes stronger and also more extensive. The separation region extends now mainly in the diverging part but also in the converging part of the channel.

Figure 10 shows the velocity field in the domain of the bubble vortex for Re = 400 and

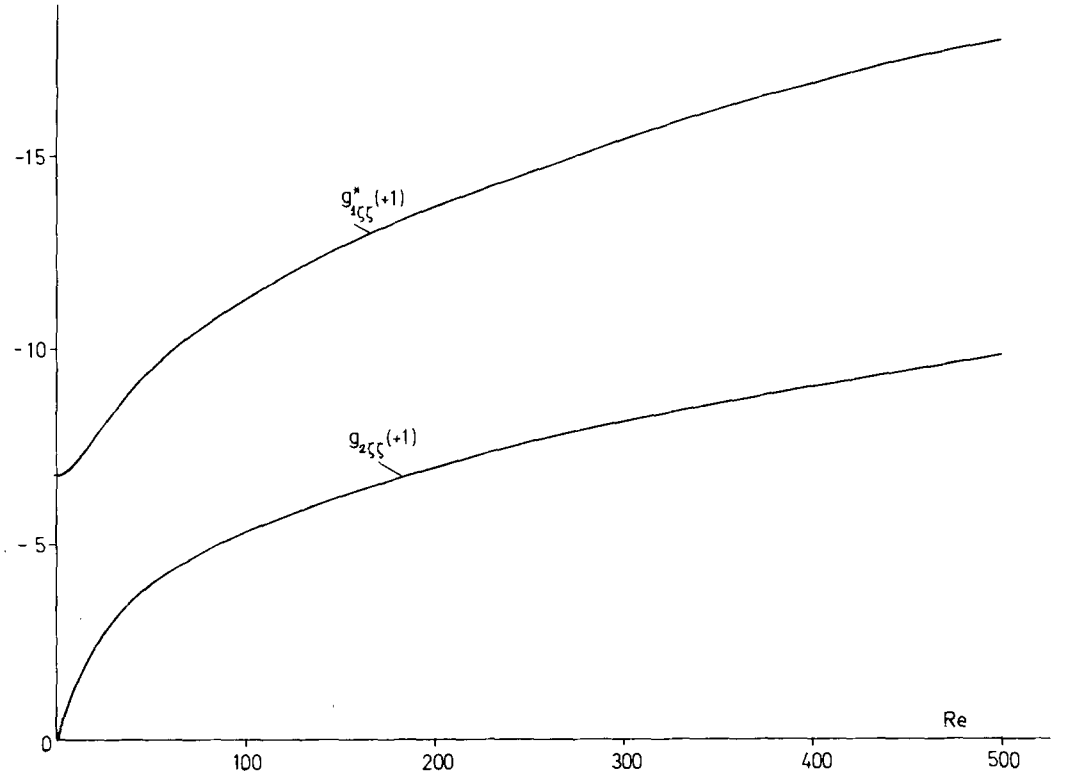

Figure 4. Variation of the second derivatives of the functions g_1^* and g_2 at the wall of the channel as functions of Reynolds number.

for a sinusoidal channel with $\epsilon = 0.3$. The center of the bubble vortex, that is the point where the velocity vanishes, can be determined. This is demonstrated in Fig. 11. In the same figure some stream lines of the velocity field are drawn. The closed stream lines have

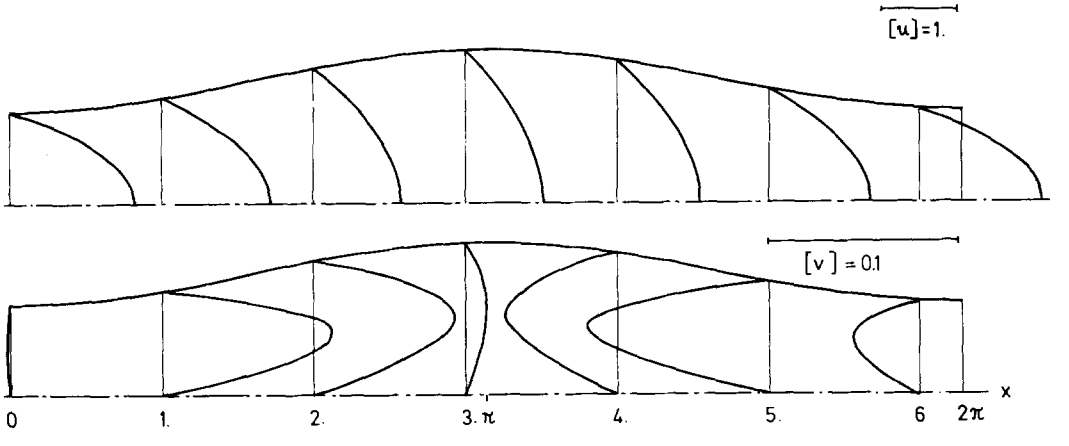

Figure 5. Longitudinal u and transversal v velocity profiles at various cross sections of the channel for a channel with $\epsilon = 0.2$ and $\mathrm{Re} = 1.0$.

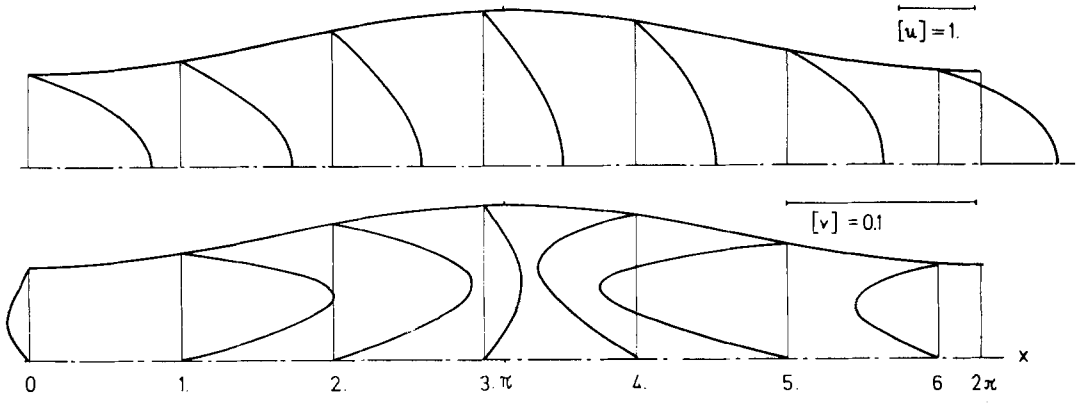

Figure 6. Longitudinal u and transversal v velocity profiles at various cross sections of the channel with $\epsilon = 0.2$ and Re = 10.0.

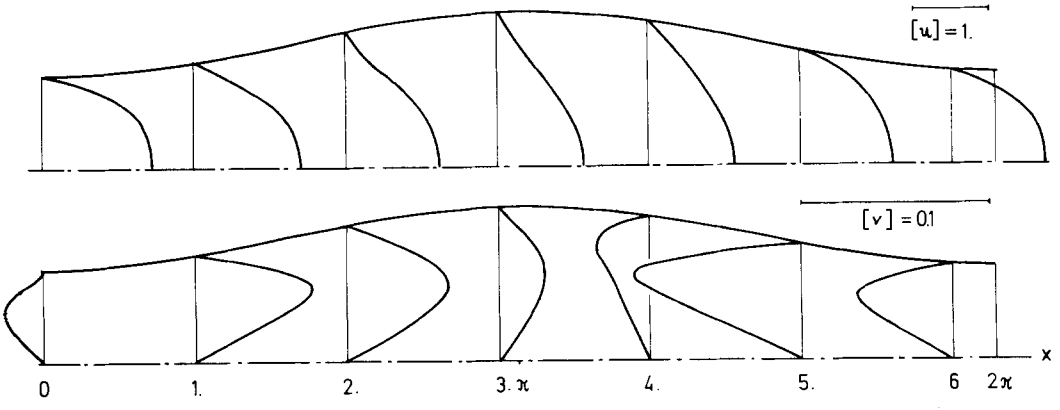

Figure 7. Longitudinal u and transversal v velocity profiles at various cross sections of a channel with $\epsilon = 0.2$ and Re = 75.

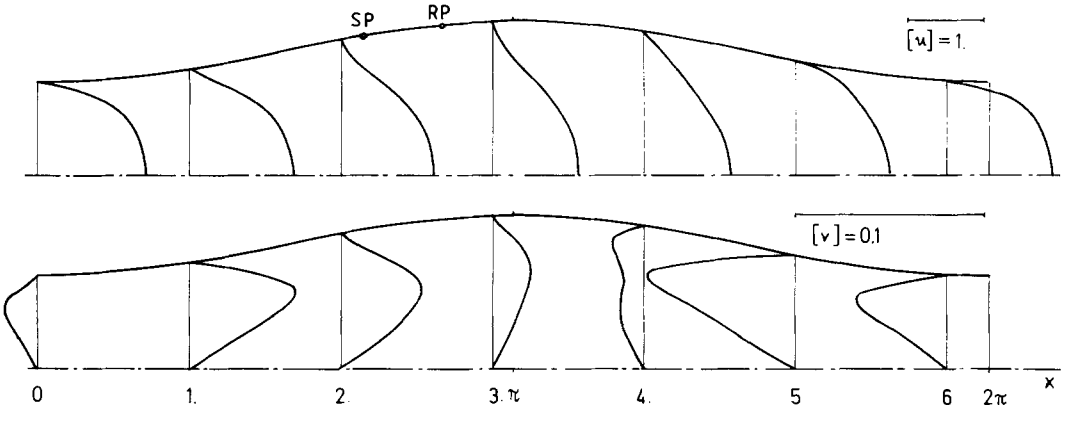

Figure 8. Longitudinal u and transversal v velocity profiles at various cross sections of a channel with $\epsilon = 0.2$ and Re = 200.

an absolute value of the stream function Ψ larger than 0.6666..., which is the value of the stream function of the solid wavy boundary. The internal boundary of the bubble vortex is limited by the second arc of the same streamline $\Psi = 0.6666....$

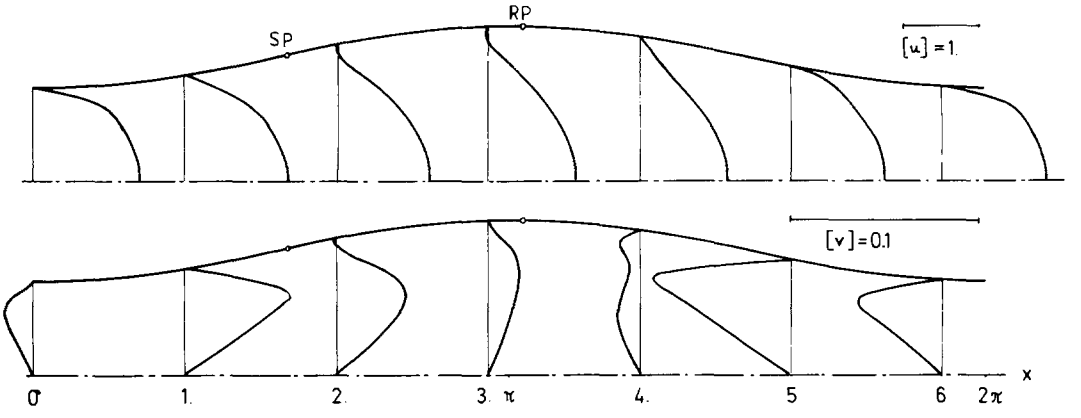

Figure 9. Longitudinal u and transversal v velocity profiles at various cross sections of a channel with $\epsilon = 0.2$ and Re = 400.

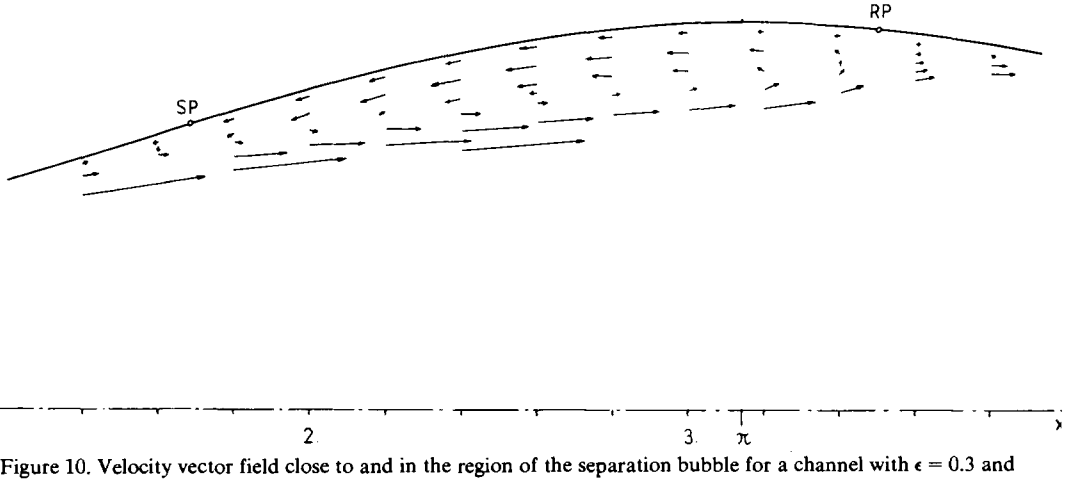

Figure 10. Velocity vector field close to and in the region of the separation bubble for a channel with $\epsilon = 0.3$ and Re = 400.

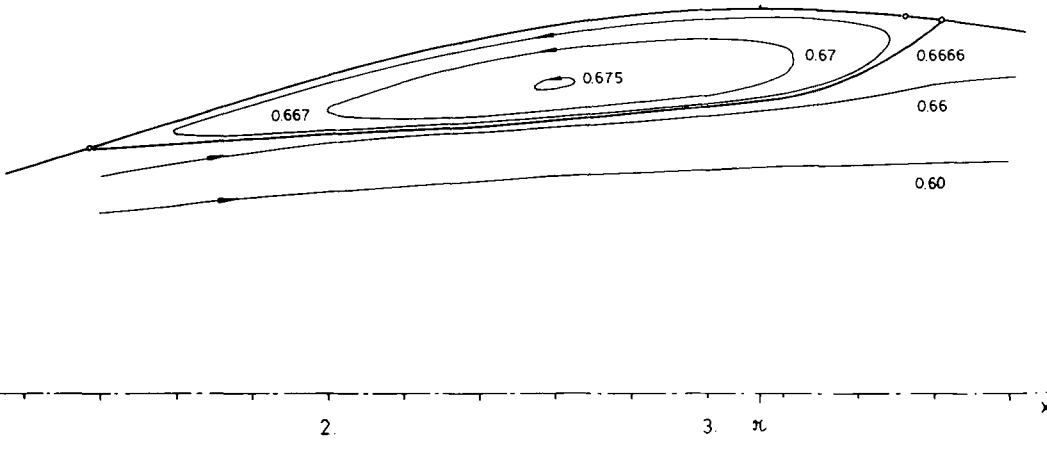

Figure 11. Stream lines close to and in the region of the separation bubble for a channel with $\epsilon = 0.3$ and Re = 400.

The shear stress is reduced to the following formula for the upper wall $\zeta = +1$:

$$\tau = \frac{(1-\epsilon^2 \sin^2\eta)^2}{[1-\epsilon(\cos\eta+1)]^2(1+\epsilon^2\sin^2\eta)}$$

$$\times\left\{-2+\epsilon\left\{\left[g^*_{1\zeta\zeta}(+1)+6\right]\cos\eta+g_{2\zeta\zeta}(+1)\sin\eta\right\}\right\}. \tag{29}$$

The term -2 within the brackets in the above equation of the shear stress is the well-known Poiseuille-term-slope in η, ζ-plane. The remaining term between the brackets is a term varying with Reynolds number. It increases by increasing the Reynolds number. Figure 12 shows skin friction τ against $\eta = x$ for three different values of the Reynolds number. The amplitude of the channel wall is $2\epsilon = 0.4$. The variation of the shear stress is a periodic function of x having a phase difference with the variation of the wall shape. Its maximum value is lying upstream of the maximum channel cross section. The amplitude of the shear stress variation at the wall increases with increasing Reynolds numbers. For Re = 25 the shear-stress variation is always negative, the flow is not yet separated. At Re = 185 separation begins on a point lying upstream of the largest width of the channel. For Re = 300 > 185 a separation region ($\tau > 0$) on the channel wall exists. By increasing the Reynolds number the separation point moves upstream and the reattachment point downstream, that means the separation region is growing with Reynolds number.

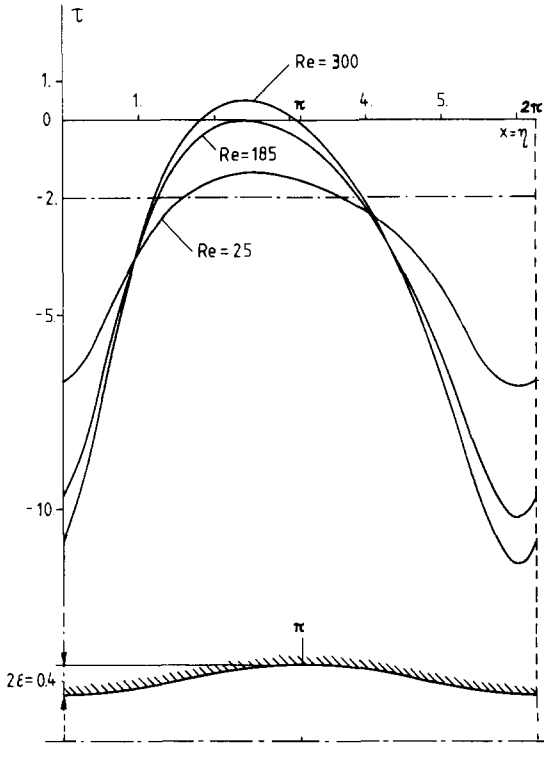

Figure 12. Shear-stress distribution for $\epsilon = 0.2$ at the upper wall $y = h(x)$, $\zeta = +1$, of the channel.

Assuming that the higher-order terms may be neglected, Eqn. (29) becomes for flow separation ($\tau = 0$):

$$0 = -2 + \epsilon \left\{ \left[g^*_{1\xi\xi}(+1) + 6 \right] \cos \eta + g_{2\xi\xi}(+1) \sin \eta \right\} \tag{30}$$

or

$$\cos \eta A + \sin \eta B = C, \tag{31}$$

where

$$A = g^*_{1\xi\xi}(+1) + 6; \qquad B = g_{2\xi\xi}(+1); \qquad C = \frac{2}{\epsilon}. \tag{32}$$

This trigonometric equation has the real solution

$$\tan \frac{\eta_0}{2} = \frac{B \pm \sqrt{B^2 + A^2 - C^2}}{A + C}, \tag{33}$$

if

$$A^2 + B^2 \geqslant C^2. \tag{34}$$

The equality $A^2 + B^2 = C^2$ yields the critical Reynolds number as a function of ϵ, i.e. that value of Reynolds number when separation appears·

$$\mathrm{Re}_{\mathrm{crit}} = \varphi(\epsilon), \tag{35}$$

and the relation

$$\eta_{0\mathrm{crit}} = \arctan \frac{B}{A} + \pi, \tag{36}$$

the position of the separation for $\mathrm{Re}_{\mathrm{crit}}$. The two points

$$\begin{aligned} \eta_{0\mathrm{sep}} &= 2 \arctan \frac{B - \sqrt{B^2 + A^2 - C^2}}{A + C} + \pi, \\ \eta_{0\mathrm{reat}} &= 2 \arctan \frac{B + \sqrt{B^2 + A^2 - C^2}}{A + C} + \pi \end{aligned} \tag{37}$$

are respectively the separation and reattachment points for

$$\mathrm{Re} > \mathrm{Re}_{\mathrm{crit}}. \tag{38}$$

Figure 13 shows how the critical Reynolds number, Eqn. (35), depends on ϵ. $\mathrm{Re}_{\mathrm{crit}}$ decreases very rapidly as ϵ increases.

Figure 14 illustrates the position of separation and reattachment points, Eqn. (37)., for some values of the amplitude parameter of the wavy channel wall.

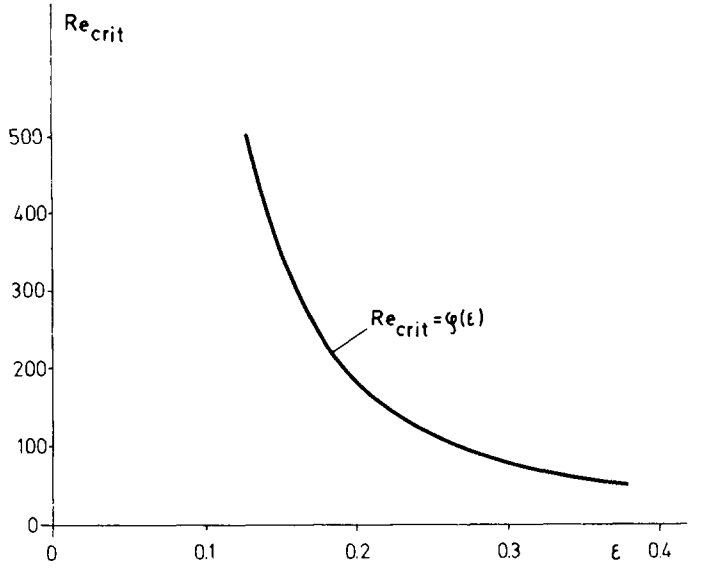

Figure 13. Variation of critical Reynolds number Re_{crit} with amplitude parameter ϵ

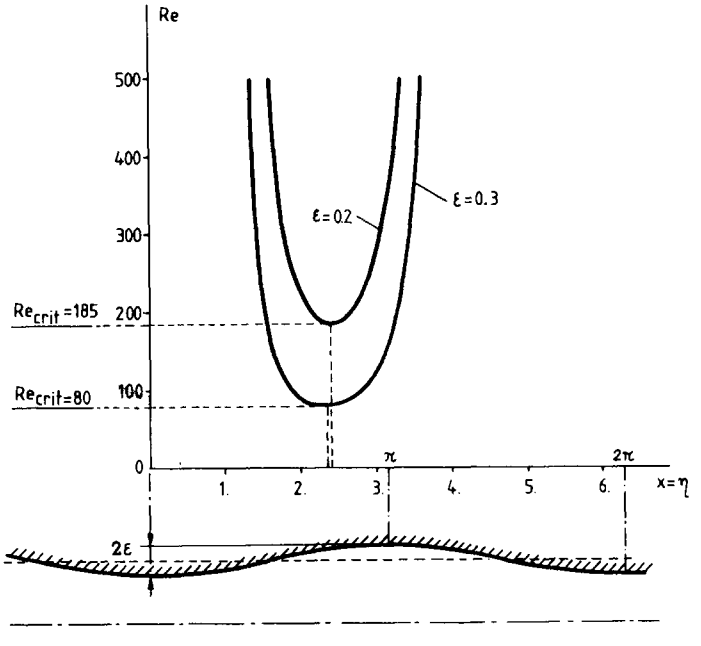

Figure 14. Position of the separation- and reattachment-points for channels: critical Reynolds numbers at the separation point and extension of the separated flow (separation and reattachment) along the wall at Reynolds numbers above critical Reynolds numbers for two different values of amplitude parameter ϵ.

5. Discussion

The comparison of the theoretical analysis of Forrester and Young [5] with subsequent experiments by the same authors (Fig. 5, p. 311) as well as the experiments by Young and

Tsai [18] (Fig. 7, p. 401) for the flow in a *stenosis* (converging-diverging *tube*) shows that the separation point for critical Reynolds number according to the theoretical curve (like that in Fig. 14) is far upstream in direction to the minimum of the tube cross section while the separation point according to experiments is nearly at the end of the stenosis. So, in the case of a separation zone ($Re > Re_{crit}$), this is also shifted downstream. The corresponding situation seems to occur with the *furrowed channel*, theoretically analysed by Sobey [10] and experimentally by Stephanoff, Sobey and Bellhouse [11].

The present results show that the separation point for critical Reynolds number lies slightly upstream the maximum width of the wavy wall of the channel (Fig. 14), and the separation regions for $Re > Re_{crit}$ are shifted downstream. Though the wall amplitude of the experiments by Stephanoff, Sobey and Bellhouse [11] is much larger, the flow features given in that paper seem to correspond at least partly with the present results. The flow in multiple stenoses as observed by Talukder et al. [15] demonstrates this effect for tubes too.

Equation (35) yields for higher Reynolds numbers a simple relation between wavy-wall amplitude ϵ and critical Reynolds number for separation:

$$Re_{crit}^{1/2}\epsilon \cong 2.75.$$

From Sobey's analysis [10] together with our assumptions for the wavy wall it turns out to be:

$$Re_{crit}^{1/3}\epsilon = 0.84.$$

The differences of the power $1/2$ respectively $1/3$ may contribute to the ongoing discussion of the generalization of Stewartson's [12], [13], [14] and Lighthill's concept of multistructured boundary layers as already pointed out by Stewartson [13] concerning scaling factors $\epsilon^3 L$ or $\epsilon^4 L$.

Acknowledgement

The authors would like to thank Dr. R. Zitny for valuable comments concerning the numerical method and for running the computer programs.

References

[1] D.C. Belinfante, On viscous flow in a pipe with constrictions. *Proceed. Cambr. Phil. Soc.* (Math. and Phil. Soc.) 58 (1962) 405–416.

[2] J.C. Burns and T. Parkes, Peristaltic motion, *J. Fluid Mech.* 29 (1967) 731–743.

[3] L.C. Cheng, M.E. Clark and W.C. Peng, The effect of oscillatory frequency in plane wavy conduit flows, *J. Biomechanics* 10 (1977) 607–609.

[4] J.C.F. Chow and K. Soda, Laminar flow in tubes with constriction, *The Phys. of Fluids* 15 (1977) 1700–1706.

[5] J.H. Forrester and Y.C. Young, Flow through a converging-diverging tube and its implications in occlusive vascular disease, Parts I and II, *J. Biomechanics* 3 (1970) 297–316.

[6] P. Hall, Unsteady viscous flow in a pipe of slowly varying cross-section, *J. Fluid Mech.* 64 (1974) 209–226.

[7] S-T. Hsu and J.F. Kennedy, Turbulent flow in wavy pipes, *J. Fluid Mech.* 47 (1972) 481–502.

[8] M.J. Manton, Low Reynolds number flow in slowly varying axisymmetric tubes, *J. Fluid Mech.* 49 (1971) 451–459.

[9] A. Ramachandra Rao and R. Devanathan, Pulsatile flow in tubes of varying cross-sections, *ZAMP* 24 (1973) 203–213.

[10] I.J. Sobey, On flow through furrowed channels. Part 1: Calculated flow patterns, *J. Fluid Mech.* 96 (1980) 1–26.

[11] K.D. Stephanoff, I.J. Sobey and B.J. Bellhouse, On flow through furrowed channels. Part 2: Observed flow patterns, *J. Fluid Mech.* 96 (1980) 27–32.

[12] K. Stewartson and P.G. Williams, Self-induced separation, *Proc. Roy. Soc.* A312 (1969) 181–206.

[13] K. Stewartson, Multistructured boundary layers on flat plates and related bodies. In: Chia-Shun Yih (ed.), *Advances in Applied Mechanics*, Vol. 14, pp. 145–239, Academic Press, New York-San Francisco-London (1974).

[14] K. Stewartson, High Reynolds-number flows. In: R. Rautmann (ed.), Approximation methods for Navier-Stokes problems, *Lecture Notes in Mathematics* vol. 771, pp. 505–518, Springer-Verlag, Berlin-Heidelberg-New York (1980).

[15] N. Talukder, P.E. Karayannacos, R.M. Nerem and J.S. Vasko, An experimental study of the fluid dynamics of multiple noncritical stenoses, *Transactions of the ASME, J. Biomechanical Engineering* 99 (1977) 74–82.

[16] S. Tsangaris and E. Leiter, Analytical solutions for weakly-stenosed channels at low Reynolds numbers, *Proc. 1st Int. Conf. Mech. Med. & Biol.* (1978) 289–292.

[17] K. Vajravelu, Fluid flow and heat transfer in horizontal wavy channels, *Acta Mechanica* 35 (1980) 245–258.

[18] D.F. Young and F.Y. Tsai, Flow characteristics in models of arterial stenoses; I. Steady flow, *J. Biomechanics* 6 (1973) 395–410; II. Unsteady flow, *J. Biomechanics* 6 (1973) 547–559.